3rd European supercritical CO2 Conference
September 19-20, 2019, Paris, France

2019-sCO2.eu-131

EXPERIMENTAL INVESTIGATION OF HEAT TRANSFER AND PRESSURE DROP IN TUBES TO COOL CO2 NEAR THE CRITICAL POINT

Andreas Wahl*
Institute of Nuclear Technology and
Energy Systems (IKE), Stuttgart, Germany
andreas.wahl@ike.uni-stuttgart.de

Rainer Mertz
Institute of Nuclear Technology and
Energy Systems (IKE), Stuttgart, Germany
rainer.mertz@ike.uni-stuttgart.de

Eckart Laurien
Institute of Nuclear Technology and
Energy Systems (IKE), Stuttgart, Germany
eckart.laurien@ike.uni-stuttgart.de

Jörg Straflinger
Institute of Nuclear Technology and
Energy Systems (IKE), Stuttgart, Germany
joerg.starfliner@ike.uni-stuttgart.de

ABSTRACT

In the frame of EU-project sCO2-flex the design of a 25 MWe supercritical CO_2 (sCO_2) Brayton cycle will be developed. The system will be optimized to meet flexibility requirements, while reducing environmental impact and focusing on cost efficiency.

In the context of a sCO_2 Brayton cycle, the gas cooler is a key component to achieve a high overall efficiency. Close to the critical point, due to varying properties, heat transfer and pressure drop of carbon dioxide (CO_2) are difficult to predict. By performing experiments with the "SCARLETT" facility of the University of Stuttgart, expertise will be gained using CO_2 as working fluid in the pseudocritical region. The results of the fundamental experiments will be used for validation and improvement of correlations to develop heat exchangers working with high efficiency.

The heat transfer and pressure drop of carbon dioxide near the critical point cooled in a 2 mm diameter was investigated. The outer wall surface temperature is determined by soldering calibrated T-type thermocouples into the copper tube wall. Thermocouples are evenly distributed along the 1.2 m cooled length. The effects of the CO_2 mass flux of 400-1400 kg/m²s, inlet pressures of 7.7-8.5 MPa, bulk fluid temperatures of 10-85 °C and the flow orientation (upward, downward and horizontal) on the heat transfer and pressure drop were examined

INTRODUCTION

A sCO_2 Brayton cycle offers a number of benefits over competing power plant cycles. A high plant efficiency can be chieved due to the favourable fluid properties in the supercritical region. This is resulting in increased electricity production with the same fuel consumption [1]. The high gas density of sCO_2 allows to reduce the necessary compressor work and leads to a reduction in the overall size of the power plant [2]. The reduced size of turbomachinery, boiler and heat exchangers can be further translated into reduced capital costs.

The moderate value of its critical pressure (7.38 MPa) makes CO_2 more economical than water where the critical point is much higher (22.1 MPa). A low heat rejection temperature leads to power cycles with high efficiencies. The critical temperature of CO_2 (31°C) contributes to that, however, it is not too low, to be cooled by the ambient temperature. CO_2 is a non-toxic and non-flammable natural working fluid ODP = 0 (ozone depletion potential) and GWP = 1 (global warming potential). It is available in sufficient quantities at reasonable costs. In environmental, cost and safety terms, CO_2 is regarded as an ideal natural refrigerant [3].

The properties of sCO_2 (Figure 1) lead to significant differences in the heat transfer characteristics [4]. This is caused by rapid changes of thermophysical properties close to the critical point. The understanding of heat transfer enhancement and deterioration phenomena during cooling in small diameter tube is crucial to develop new concept of compact heat exchanger for the Brayton cycle able to work with high efficiency, speed and reliability under high CO_2 pressure and low pinch point. The thermophysical properties change strongly with temperature and pressure.

As shown in Figure 1, for each pressure (77bar, 81 bar and 85 bar), the viscosity and density are strongly decreasing with increasing temperature. The isobaric heat capacity and thermal conductivity pass through a peak crossing the pseudocritical temperature. The pseudocritical temperature increases with increasing pressure [5]. Moreover, the distinct peaks are flattened.

In this study, the heat transfer and pressure drop in cooling conditions were measured at different CO_2 pressures, mass fluxes, temperatures and flow orientations. The effects of the parameters on the heat transfer were demonstrated. The measured pressure drop was compared with the prediction by taking in to account bulk, film and wall fluid properties.

* corresponding author(s)

10.17185/duepublico/48882

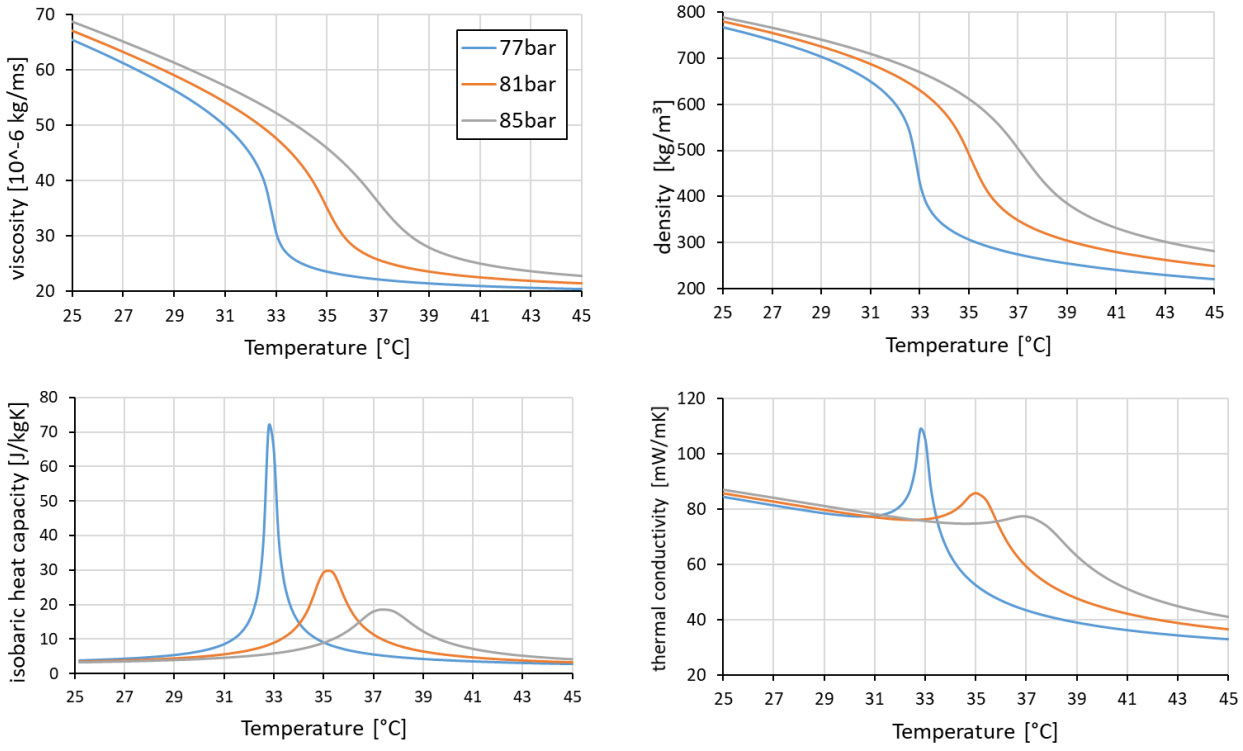

Figure 1: Properties of CO2 vs temperature at different pressure [4]

STATE-OF-THE ART OF COOLING HEAT TRANSFER EXPERIMENTS

A number of researchers have experimentally investigated the heat transfer and pressure drop performance of CO_2 in tubes of different sizes and flow orientations. The research has been concentrated on tubes ranging from 0.5 to 10.7 mm in upwards, downwards and horizontal flow. Most of the work have been carried out in horizontal orientation.

Dang and Hihara [8] investigated the heat transfer and pressure drop in tubes with four different diameters ranging from 1 to 6 mm. The temperature of the outer tube wall was measured at 10 locations equally distributed along the 500 mm long tube-in-tube counter-flow heat exchanger. They found, that the Nusselt number increases slightly with increasing tube diameter. The comparison of the heat transfer coefficient over the bulk and film fluid temperature showed that the maximum is reached when the film temperature reaches the pseudocritical temperature. The film temperature is defined as:

$$T_f = \frac{(T_b + T_w)}{2} \tag{4}$$

The result is a modified Gnielinski equation [9] taking the film properties into account:

$$Nu_f = \frac{\left(\frac{f_f}{8}\right)(Re_b - 1000)Pr}{1{,}07 + 12{,}7\sqrt{\frac{f_f}{8}}\left(Pr^{\frac{2}{3}} - 1\right)} \tag{5}$$

The Prandtl Number is defined with a variation in three different cases [8]. Due to large variations of thermophysical properties within a small temperature range, the heat transfer of supercritical fluid flow is strongly affected by heat flux and flow direction. Jackson and Hall [10] have developed a semi empirical parameter to characterize the influence of natural convection on turbulent vertical flows.

$$\frac{Gr}{Re^{2.7}} > 10^{-5} \tag{6}$$

In the case of cooling heat transfer, the turbulent upward flow leads to an intensification of heat transfer. The turbulent aiding mixed convection is present when the free and forced convection are in opposite direction. In the downward flow, a strong degradation of heat transfer is observed. In this case, the free and forced convection flows are in the same direction [11].

10.17185/duepublico/48882

EXPERIMENTAL SET-UP

The test section applied here consists of a 1.5 m long cooper tube. The inner tube diameter is 2 mm and the outer tube diameter is 6 mm. The CO_2 flow can form a fully developed turbulent flow in the first 57 mm of the tube. At this point, a 1 mm hole is drilled through the tube wall to measure the pressure with relatively small impact on the flow. Additional 93 mm of uncooled tube length follows. The total cooled length of the tube is 1200 mm. The total length of the differential pressure measurement is 1386 mm, which contains an uncooled length of 186 mm (Figure 2).

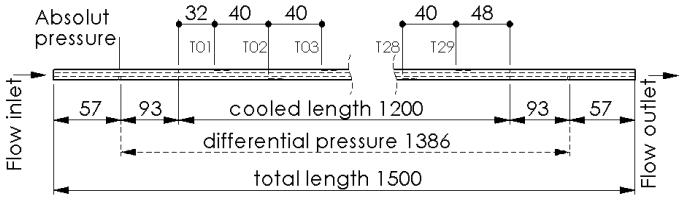

Figure 2: Detailed view of the test tube

T-type thermocouples are soldered into milled channels on the surface of the tube (Figure 3). The thermocouples are coated with stainless steel leading to high durability against corrosion. The heat conductance in the thermocouple wire could lead to a measurement error, thus the thermocouples have to be embedded a certain length inside the tube to eliminate this influence. The T-type thermocouples have a diameter of 0.5 mm. They are bended and laid in the milled channels (0.8x0.8x8mm depth/ width/length).

The bending of the thermocouple leads to an asymmetry of the temperature measurement points in the cooled length. The first measurement position (T_{01}) is at 32mm of the cooled length. The spacing is equal along the tube with 40 mm between the measurement positions. The thermocouples were placed alternating on the top and on the bottom of the tube, to be able to investigate flow stratification. The solder alloy used to connect the tube with the thermocouples was a 96 % tin and 4 % silver mixture with implemented colophony. This material has a low temperature melting point (Solidus: 221 °C, Liquidus 238 °C), which does not exceed the temperature range of T-type thermocouples (-40 °C…+350 °C) and leads to a good thermal connection of the two components due to the high thermal conductivity.

The “outer tube” was designed to lead the thermocouples to the inner tube, deliver the cooling media in-and outflow, and close the annulus stream leak-tight .

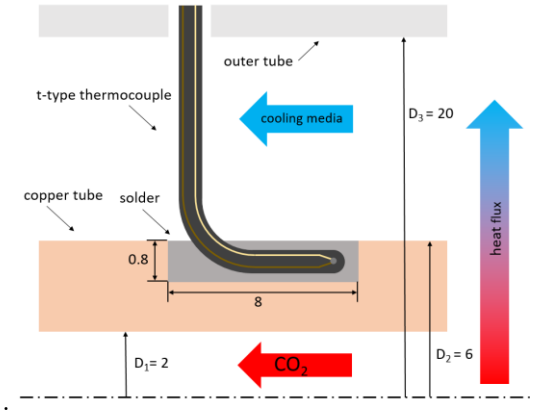

Figure 3:Detailed view of the thermocouple soldering in the tube surface (All dimensions in mm)

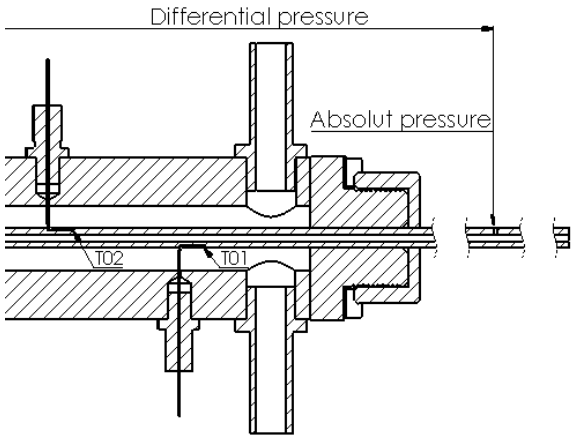

Figure 4: Flanging and cooling media supply into the test section

The flanges center the tube in the annulus. The size of the annulus is capable to deliver a high volume flux of cooling media (Figure 4). This intends to reduce the temperature difference in the flow, thus to support the inner tube with an isothermal cooling media. That could reduce the complexity and inaccuracies of the experiments.

The two before mentioned authors focused on the axially-averaged heat transfer. In Liao and Zhao’s [6] study, using a tube diameter of 2.1 mm and a 110 mm test section the heat transfer coefficient was averaged along a length to diameter ratio of 157. For Dang and Hihara’s [8] 2 mm tube, this value was 250. With the test facility presented in this work, the influence of CO_2 mass flow rate, CO_2 bulk fluid temperature, CO_2 pressure, volumetric cooling media flow and cooling media temperature can be investigated with a length to diameter ratio of 20, resulting in a higher resolution.

The SCARLETT test loop provides sCO_2 under defined boundary conditions. Figure 5 depicts the piping and instrumentation (P&I) diagram of the SCARLETT test loop, which is described as follows [12]. After evacuating the loop with a vacuum pump, the pressure vessels (1, 10) are filled with

10.17185/duepublico/48882

CO_2 by a gas bottle. During normal operation, liquid CO_2 flows from the pressure vessel 1 through an electrical heated evaporator (2) and is slightly superheated. After leaving a demister unit (3), where remaining liquid CO_2 is separated from the flow, it enters a compressor (4), where it is compressed to a certain pressure and simultaneously heated by the compression.

Before entering a test section, there is a conditioning (5) of the sCO_2, which means that a defined temperature can be adjusted via cooling or heating the sCO_2 mass flow rate. In the test-section (6) different kind of experiments can be performed. After leaving the test section, the sCO_2 is cooled down in a gas cooler (7) followed by the expansion in an expansion valve (8). Before it enters the pressure vessel 2 (10) the CO_2 can be cooled down again in a condenser (9). Finally, it is pumped back from the pressure vessel 2 into the pressure vessel 1. The sCO_2 mass flow rate in the SCARLETT test loop can be adjusted from about 30 to 110 g/s. Lower mass flow rate in the test section can be achieved by bypassing with needle valves. It must be mentioned, that the achievable mass flow rate depends on the compressor performance map, which leads to less mass flow rate at higher pressures and vice versa. The sCO_2 temperature at the inlet of the test section can be varied from about 0 to 140 °C and the pressure from about 75 to 110 bar.

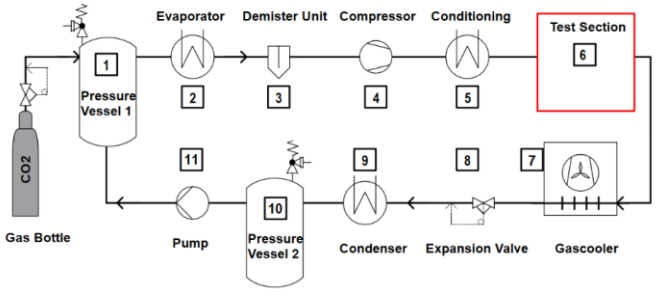

Figure 5: P&I diagram of the SCARLETT test loop.

DATA REDUCTION

All thermophysical properties were calculated using the Software REFPROP ver.9.0 [4]. The Reynolds numbers of the CO_2 flow are determined by measuring the CO_2 mass flow rate $\dot{m}_{CO2}$ by a Coriolis flowmeter. At the inlet, the dynamic viscosity (η_{CO2}) of the flow can be calculated as a function of measured pressure (P_{CO2}) and temperature (T_{CO2}). Due to the varying thermophysical properties, the Reynolds number decreases drastically by crossing the pseudocritical temperature. Reynolds number at inlet conditions is calculated by:

$$Re_{CO2} = \frac{4\dot{m}}{\pi d \eta} \tag{7}$$

The heat input $\dot{Q}$ at each discretization step was defined by the calculated heat transfer coefficient htc_{cool}, the outer tube area $A_{t,o}$ and the temperature difference between wall and cooling media temperature.

$$\dot{Q} = htc_{cool} * A_{t,o} * (T_{t,o} - T_{cool}) \tag{8}$$

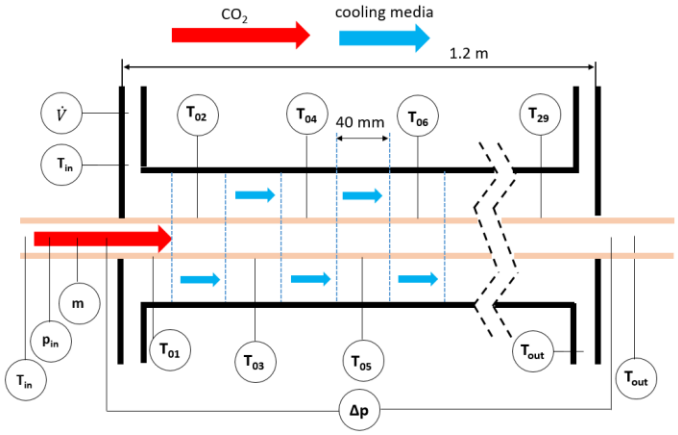

Figure 6: Schematic diagram of the test section including all measured quantities

The heat transfer coefficient of the cooling media flow in the annulus was estimated by the Nusselt correlation of Dirker [13]. htc_{cool} was assumed to be equal along the test section of 1200 mm. This assumption could lead to an overestimation of the CO_2 temperature along the tube by underestimating the heat flux in the entrance area of the cooling media flow. The described behaviour of the cooling media flow will be investigated in an additional test facility to implement a function of htc_{cool} over the length of the test section.

$$htc_{cool} = f(\dot{V}_{cool}, d_i, d_o, \text{fluid properties}) \tag{8}$$

The heat transfer through the copper tube $\dot{Q}$ leads to a small difference between the inner ($T_{t,i}$) and outer ($T_{t,o}$) temperature of the tube wall by taking into account the thermal conductivity λ_{Cu}, the inner and outer diameter of the test tube (d_o, d_i), the length of the pipe section L.The inner tube temperature $T_{t,i}$ is equal to the wall temperature of CO_2 $T_{CO2,w}$.

$$\dot{Q} = \frac{2\,\pi\,L\,\lambda_{Cu}}{\ln(\frac{d_o}{d_i})}\,(T_{t,o} - T_{t,i}) \tag{9}$$

The heat transfer coefficient at the bulk temperature of CO_2 at every discretisation step was calculated by the heat $\dot{Q}$, the inner tube area A_i and the temperature difference between bulk and wall temperature.

$$htc_{CO2} = \frac{\dot{Q}}{A_i * (T_{CO2,b} - T_{CO2,w})} \tag{10}$$

Both, CO_2 and cooling media temperatures are measured at the in- and outlet. Within the tube, the temperatures are calculated by the heat flux of the previous discretization step and the respective mass flux to determine the enthalpy of the flow. The heat exchanger is operated in co-current flow.

$$h_{CO2/cool}(x+1) = h_{CO2/cool}(x) \pm \frac{\dot{Q}(x)}{\dot{m}_{CO2/cool}} \tag{11}$$

The procedure leads to 29 sets of the process parameters along the test section. Each thermocouple measurement is paired

10.17185/duepublico/48882

with a cooling media and a CO_2 temperature. The calculation leads to a progress of the CO_2 bulk fluid temperature, which is the result of the earlier described assumptions, all parameters measured at the inlet and most significantly, the properties of CO_2.

UNCERTAINTY ANALYSIS

The uncertainty was mainly caused by the heat flux prediction by a uniform htc_{cool} along the test section and the temperature measurements. Prior to installation, the thermo-couples were calibrated within a range of 5-60 °C by the use of a high accurate reference RTD (calibrated to 0.02 K). The resulting accuracy of the T-type thermocouples was ±0.1 K. The RTD's to measure both flows at in and outlet were ±0.3 K. The accuracy of the pressure transducer was 0.15 % of full range of 3/100 bar. The accuracy of the Coriolis-type mass flow meter was assumed to be 0.3 %. The volume flux of the cooling media was measured using an electromagnetic flow meter. The measurement data acquisition was used with a 40-channel Armature Multiplexer and a terminal block with temperature reference.

Additional to the measurement errors, the error of the manual soldering process has to be taken into account. For example, the manufacturing inaccuracies of the milled channels, the placing in the channel and the properties of the solder contribute to the assumed accuracy of the outer wall temperature of the cooper tube ($T_{t,o}$) of ±0.2 K.

htc_{cool} was assumed be constant along the test section with an accuracy of ±20 %. This value is a coarse estimation up to now. A 3-D flow simulation is planed to validate this assumption.

Due to the explained assumptions, the accuracy of the CO_2 temperature along the test section was assumed as ±0.5 K. From manufacturer certificate, the error of the inner and outer tube diameter was 0.05 mm. The heat conductivity of the cooper tube λ_{Cu} was assumed as 340 W/mK ±40 W/mK.

Table 1: Measured quantities and achieved accuracies

Meas. quantity	Symbol	Range	Unit	Accuracy
Volumetric flow	$\dot{V}$	0-2.5	l/s	±1%
Mass flow rate	$\dot{m}$	0-50	g/s	±0.3%
Pressure	P	0-100	bar	±0.15
Diff. pressure	ΔP	0-3000	mbar	±4.5
Thermocouples	T	5-60	°C	±0.1
RTD	T_{in}/T_{out}	0-100	°C	±0.3

RESULTS AND DISCUSSION

In this experimental study, the heat transfer was derived for different boundary conditions (Table 2). In Table 3, the measurement campaigns are summarized. The isothermal measurements were conducted with no cooling media flowing in the annulus.

Table 2: Experimental inlet conditions: horizontal cooling

CO_2		
Temperature [°C]	Pressure [bar]	Mass flux [kg/m²s]
37-85	77-85	400-1400

Cooling media	
Temperature [°C]	Volumetric flow [l/s]
10-25	0.1-0.2

Table 3: Measurement campaigns

condition	Flow direction	Number of experiments
isothermal	horizontal	91
cooled	horizontal	64
cooled	upwards	25
cooled	downwards	18

EXPERIMENTAL SYSTEM VALIDATION

The calculated results of the CO_2 heat output Q_{CO2} are shown in Figure 7 as a function of the calculated cooling heat input $\dot{Q}_{cool}$ in order to validate the experimental system. The results show that the heat transfer is mainly within range of ±20%. The uncertainties result from the temperature measurements. The small temperature difference (1-3 K) in the cooling media flow leads to a relatively high error of these values. In general, the calculated cooling media heat input is higher than the CO_2 heat output. At lower cooling media temperature, the behaviour seems to increase.

10.17185/duepublico/48882

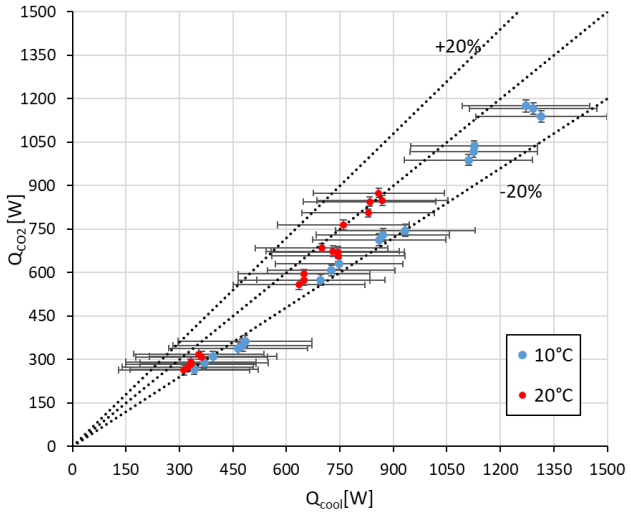

Figure 7: Energy balance: Q_{sCO2} as a function of Q_{cool}

Figure 8 shows the result of a measurement point including error bars. htc_{CO2} is displayed as a function of the bulk fluid temperature. The experimental conditions were $\dot{m}$ = 2.7 g/s CO_2, which is equal to a mass flux of G = 860 kg/m²s for the inner tube diameter of 2mm. The volumetric cooling media flow rate was 0.1 l/s. The inlet conditions on the CO_2 side were 77 bar, 81.4 °C and Re = 88400. The inlet temperature of the cooling media was 10.2 °C.

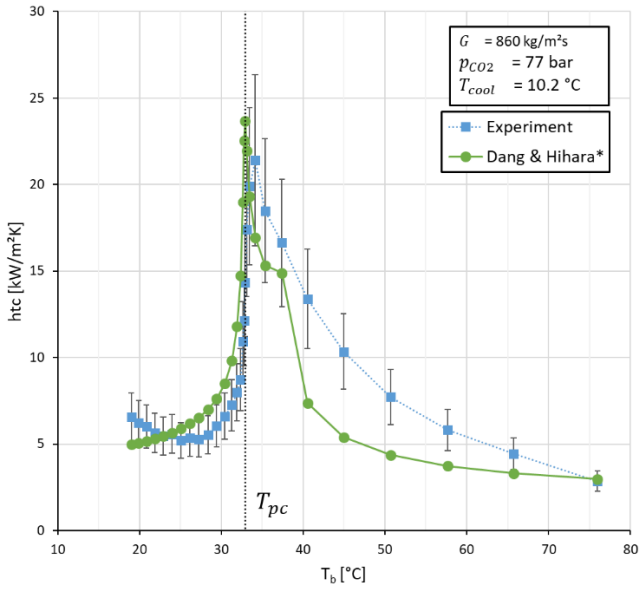

Figure 8: Heat transfer coefficient over bulk temperature at m= 2.7g/s, G = 860 kg/m²s and p_{CO2}= 77 bar

Due to the heat flux, CO_2 temperature is decreasing while cooling media temperature is increasing. The Reynolds number drops by the factor of 3. This is caused by the increase of viscosity.The results show a distinct peak close to the pseudo critical temperature (dashed line). The results are comparable with the predicted values of the Dang and Hihara [8] correlation.

EFFECT OF MASS FLUX

Figure 9a) presents the effect of mass flux at 415, 830 and 1370 kg/m²s (1.3, 2.6 and 4.3 g/s) for p_{CO2} = 85 bar and T_{cool} = 10 °C. The heat transfer coefficient is shown as a function of T_b. The htc increases as the mass flux increases due to an increase in turbulent diffusion. As shown by Dang and Hihara [8], the maximum htc occurred at T_b slightly higher than T_{pc}.

In Figure 9 b) the heat flux q_{CO2} is shown as a function of T_b. The heat flux is in total higher for increased mass flux. This is caused by the increased htc_{CO2} , whereas T_{cool} and htc_{cool} were constant. The heat flux underwent a sharp decrease by crossing the pseudocritical temperature. At the first position of temperature measurement. q_{CO2} is lower than the second position due to the lower temperature caused by heat conduction towards the flanging.

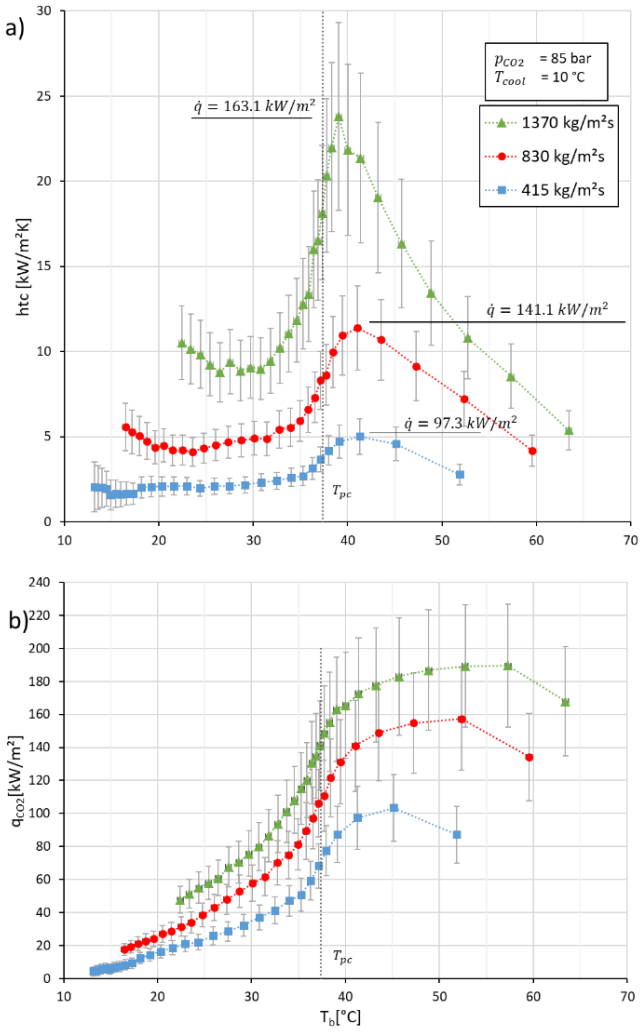

Figure 9: htc and heat flux over bulk temperature for different mass fluxes at p_{CO2} = 85 bar and T_{cool} = 10 °C

10.17185/duepublico/48882

In Figure 10 the htc is displayed at p_{CO2} = 81 bar and T_{cool} = 20 °C for different mass flux as a function of a) T_b and b) T_f. The peak in the heat transfer is located at the same bulk temperature for all mass fluxes. Depending on the film temperature, the temperature of the peak value seems to increases with increasing mass flux. This finding is contrary to Dang and Hihara's [8] work. It is to mention here that they showed this relation at a constant cooling heat flux of 12 kW/m² on a 4 mm tube. Further testing is necessary to achieve a better comparability. This will include higher temperature of the cooling media to achieve lower cooling heat flux.

The influence of the mass flux on the heat transfer coefficient increases near the critical temperature. When the mass flux was increased by a factor of 2, htc_{CO2} increased by a factor of about 1.6 in the early stage of the cooling process whereas by a factor of about 3.3 near the critical point

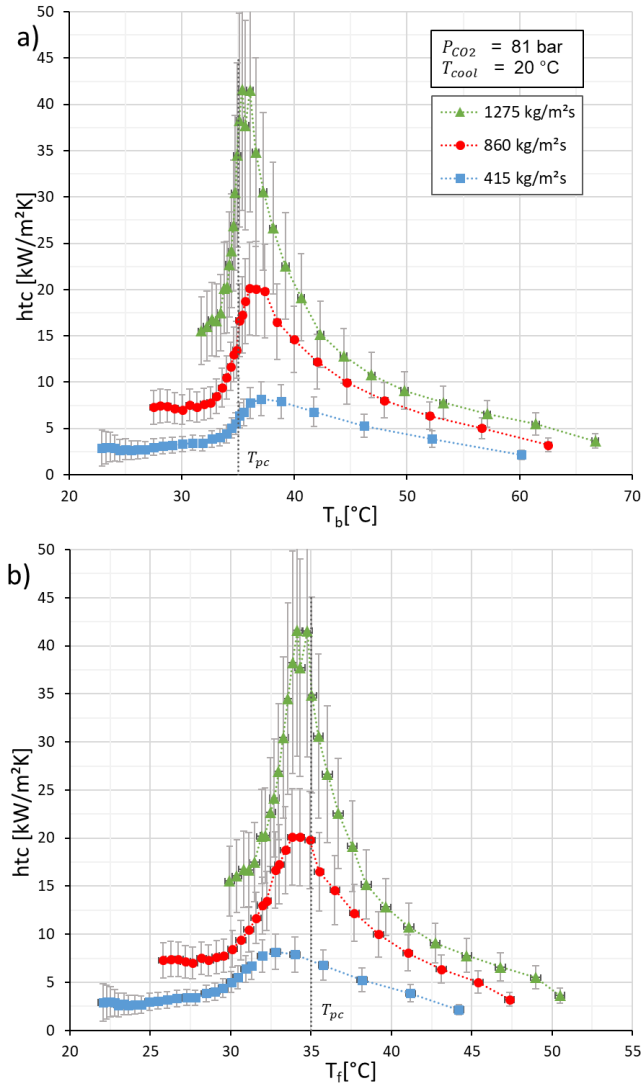

Figure 10: htc over bulk- and film temperature for different mass flux at p_{CO2} = 81bar and T_{cool} = 10 °C

EFFECT OF INLET PRESSURE

Figure 11 presents the htc of CO_2 for three different pressures ranging from 77 bar to 85 bar at G = 860 kg/m²s and T_{cool} = 10°C. For each pressure, the htc shows the same tendency in the gas like region. The htc increases continuously by approaching the pseudocritical temperature. In this stage, higher pressure has higher heat transfer coefficient due to the higher specific heat. The htc peak values are damped and moved to higher temperature with increased pressure. htc-values of 21, 15 and 12 kW/m²s are reached, respectively. This behaviour is related to the evolution of specific heat with temperature and pressure as shown in Figure 2. In the liquid-like region of the cooling process, the htc decreases for all pressures to the same level. In this stage, higher pressure has lower heat transfer coefficient due to the lower specific heat. The increasing tendency of the htc in the late stage of the cooling process, below T_b = 25 °C in this case, is under investigation yet. In this temperature range, however, the measurement uncertainty increases as the CO_2 temperature approaches the cooling media temperature.

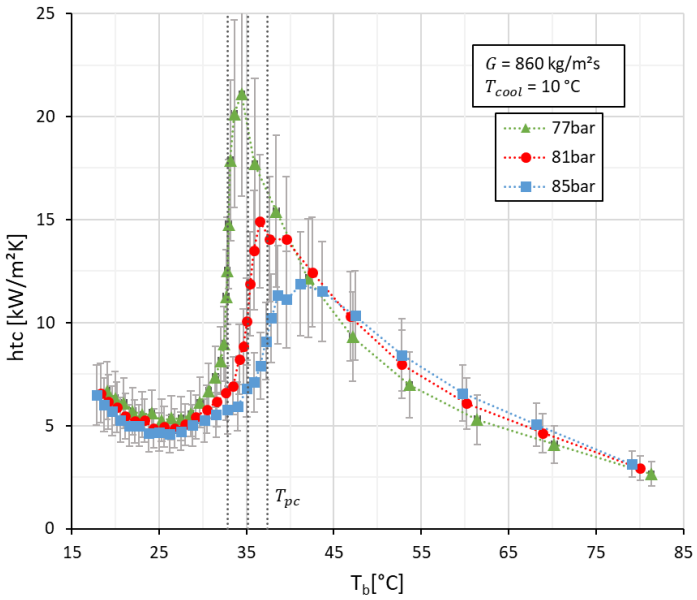

Figure 11: htc over bulk temperature for different pressures at G = 860 kg/m²s and T_{cool} = 10°C

10.17185/duepublico/48882

EFFECT OF COOLING MEDIA TEMPERATURE

Figure 12 a) shows the htc at two different cooling media temperatures at p_{CO2} = 77 bar, G = 860 kg/m²s. T_{cool} = 20 °C leads to slightly lower htc in the early stage of the cooling process whereas the peak value is significantly higher. In the late stage of the cooling process, the tendency is reversed: higher cooling media temperature leads to a higher htc.

In Figure 12 b) the wall temperature is displayed as a function of the bulk fluid temperature. T_{cool} = 10 °C leads to a lower wall temperature, thus, the wall temperature is subcritical from the early stage of the cooling process. As T_b approaches T_{pc}, T_w is already far below T_{pc}, thus, the wall properties left the beneficial temperature range, which is close to the pseudocritical critical temperature.

At T_{cool} = 20 °C, the wall temperature reaches the pseudocritical temperature at T_b = 48 °C. As T_b reaches T_{pc}, T_w is close to T_{pc}. Thus, both T_b and T_w are in the temperature range of beneficial properties.

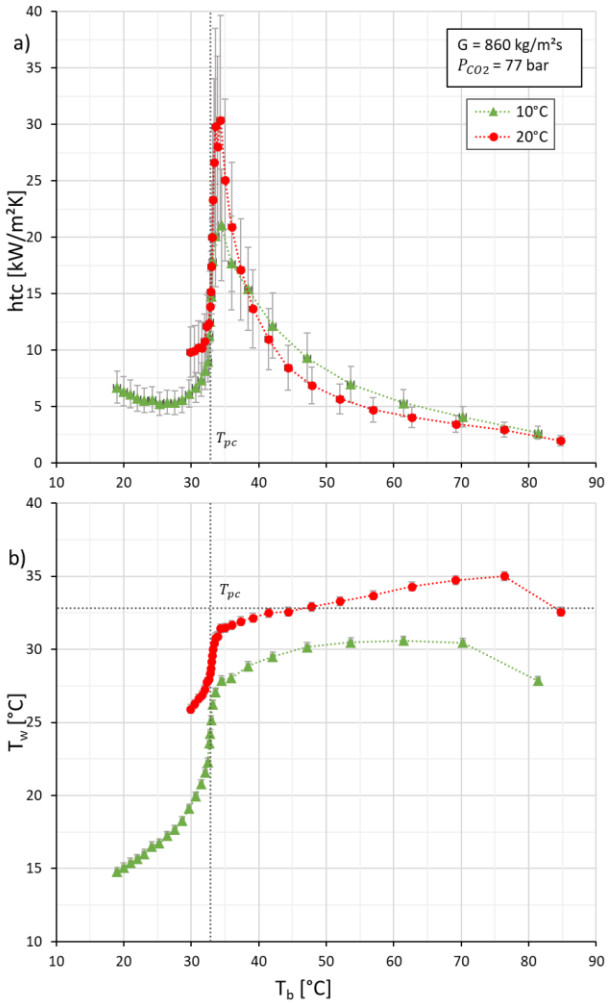

Figure 12: htc and Tw over bulk temperature for different cooling media temperature atG = 860 kg/m²s and p = 77bar.

EFFECT OF FLOW DIRECTION

Figure 13 a) shows the htc for up- and downwards flow at p_{CO2} = 80 bar, G = 415 kg/m²s and T_{cool} = 25°. Figure 13 b) illustrates the mixed convection parameter $Gr/Re^{2.7}$. The horizontal dotted line displays the limit value defined by Jackson and Hall [10]. The mixed convection parameter increases in the gas like region towards a maximum value at the pseudocritical temperature. A sharp decrease is present in the liquid like region.

The mixed convection parameter at the presented configuration of 415 kg/m²s, resulting in $Re_{CO2,in} = 42000$ and $Re_{CO2,out} = 13000$, is reaching the limit value near the pseudocritical point. However, does not exceed this value significantly. As the htc for up-and downwards flow show no significant difference, the limit value can be confirmed as far as, that at values up to 10^{-5} no influence present.

To reach higher values of the mixed convection parameter to investigate enhancement and degradation phenomena the mass flux has to be further reduced or the tube dimeter has to be increased.

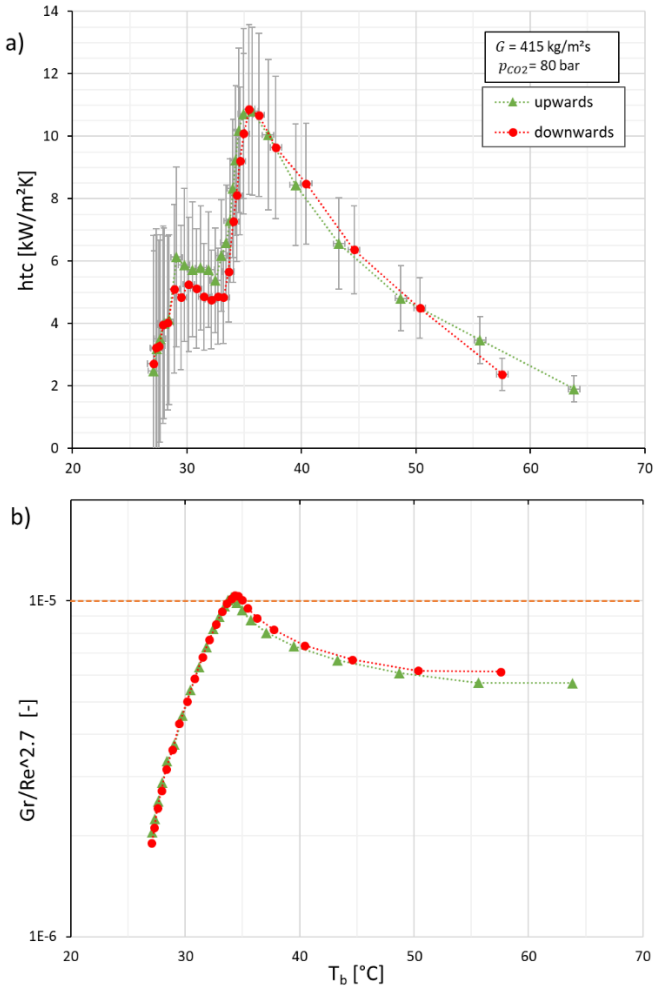

Figure 13: htc and Gr/Re^2.7 over bulk temperature for different flow orientations at ṁ = 1.3 g/s and p = 80bar.

10.17185/duepublico/48882

PRESSURE DROP

Frictional pressure drop in fully developed turbulent single phase flow is calculated by taking into account the length of the test section l, mass flow rate $\dot{m}$, inner diameter d and the density ρ at the present pressure and temperature.

$$\Delta p = \zeta \frac{l}{d} \frac{\rho v^2}{2} = \frac{8}{\pi^2} \zeta \frac{l \dot{m}^2}{d^5 \rho} \quad (12)$$

The dimensionless friction factor ζ can be predicted as a function of Reynolds number Re and the relative roughness $\varepsilon = K/d$ with the roughness of the wall K [14].

$$\frac{1}{\sqrt{\zeta}} = -2\, lg \left[\frac{2.51}{Re \sqrt{\zeta}} + \frac{K/d}{3.71} \right] \quad (13)$$

The roughness of the tube was measured at three samples. The average value of 18.1 μm was taken into account to predict the friction factor. Figure 14 presents the friction factor of the uncooled flow in comparison with the presented prediction.

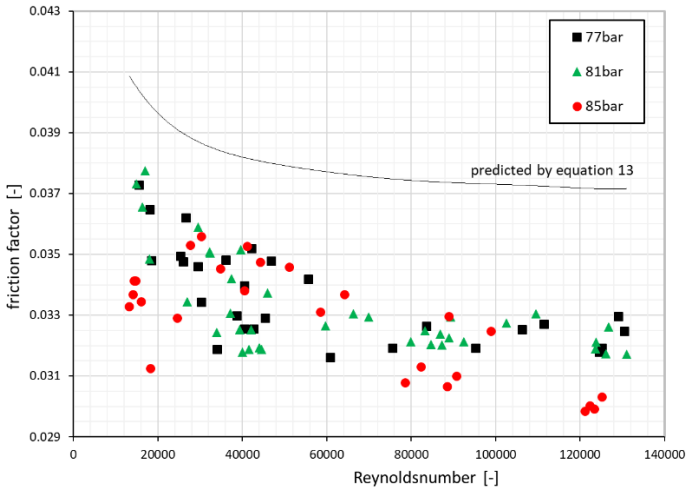

Figure 14: friction factor of the uncooled flow compared with the predicted value

The results show no significant difference for the three operation pressures. The evolution of the predicted value can be reproduced. At higher Reynolds number, the friction factor of rough pipes becomes constant, depending only on the pipe roughness as predicted by the moody chart [14]. The average deviation is 14%.

The prediction of the pressure drop under cooling conditions is shown in Figure 15. The predict was conducted by taking in to account the bulk, film or wall fluid properties. The prediction by the bulk fluid properties shows the highest error. The prediction with film and wall fluid properties show a much better agreement mainly within an error of 20%

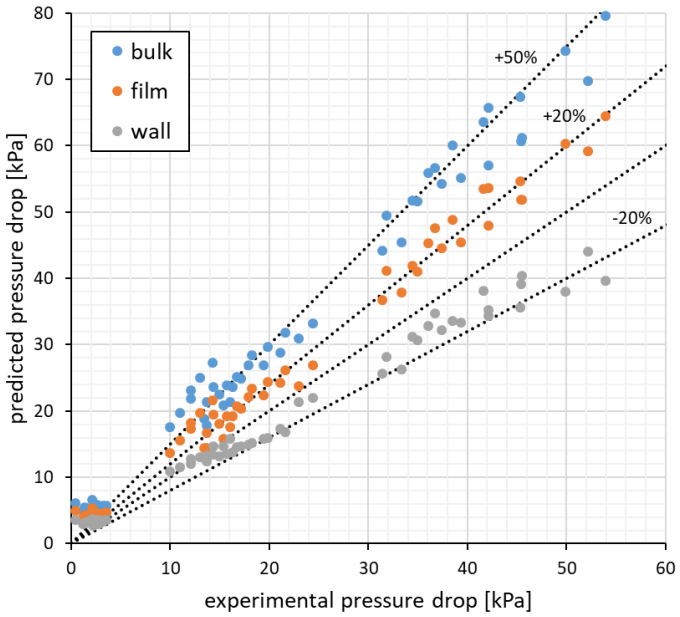

Figure 15: Experimental versus predicted pressure drop for different fluid

CONCLUSIONS

The cooling heat transfer of CO_2 near the critical point was investigated. Significant effects of mass flux, inlet pressure and cooling media temperature on the heat transfer were analysed. The mass flux showed significant effect especially near T_{pc}. The peak value of htc_{CO2} appeared at T_b slightly higher than T_{pc}. Lower cooling media temperature caused stronger sub cooling, which leads to a lower peak value of htc_{CO2}.

The influence of the flow orientation on the heat transfer coefficient is negligible within the investigated parameter range. However, the limit value of the mixed convection parameter was confirmed in this study. At $Gr/Re^{2.7} < 10^{-5}$ no difference between up and downwards flow is present.

The pressure drop in the isothermal experiments were predicted with an average error of +14%.

The prediction under cooling condition showed a much better agreement by taking into account the fluid conditions of the film and wall.

10.17185/duepublico/48882

NOMENCLATURE

A	(m^2)	area of heat transfer
c_p	(J/kgK)	specific heat
g	(m/s^2)	acceleration of gravity
G	(kg/m^2s)	mass flux
Gr	(-)	Grashof number
h	(kJ/kg)	spec. Enthalpy
htc	(W/m^2K)	heat transfer coefficient
K	(m)	wall roughness
L	(m)	length of discretization
$\dot{m}$	(kg/s)	mass flow rate
Nu	(-)	Nusselt number
P	(bar)	pressure
Pr	(-)	Prandl number
Q	(W)	heat
Re	(-)	Reynolds number
T	(°C)	temperature
v	(m/s)	velocity
V	(l/s)	volumetric flow

Greek symbols

Δp	(bar)	pressure drop
ε	(-)	relative roughness
η	(kg/ms)	dynamic viscosity
λ	(W/mK)	heat conductivity
ρ	(kg/m^3)	density
ζ	(-)	friction factor

subscripts

b	bulk
cool	cooling media
corr	correlation
CO_2	carbon dioxide
Cu	copper
exp	experiment
f	film
in	inlet
out	outlet
t	tube
w	wall

ACKNOWLEDGMENT

This project has received funded by the European Union's Horizon 2020 research and innovation programme under grant agreement No 764690

REFERENCES

1. C. M. Mendez and G. Rochau, "sCO2 Brayton Cycle: Roadmap to sCO2 Power Cycles NE Commercial Applications -SAND2018-6187", *Albuquerque, New Mexico*.
2. V. Dostal; M. J. Driscoll; P. Hejzlar, "A Supercritical Carbon Dioxide Cycle for Next Generation Nuclear Reactors", *Advanced Nuclear Power Technology Program*, *MIT Center for Advanced Nuclear Energy Systems*, pp. 1–326 (2014).
3. S. B. Riffat; C. F. Afonso; A. C. Oliveira; D. A. Reay, "Natural refrigerants for refrigeration and air-conditioning systems", *Applied Thermal Engineering* 1, pp. 33–42 (1997).
4. E. W. Lemmon, M. L. Huber, M. O. McLinden, *REFPROP*, NIST SRD 23, United States of America (2010).
5. L. F. Cabeza; A. de Gracia; A. I. Fernández; M. M. Farid, "Supercritical CO2 as heat transfer fluid: A review", *Applied Thermal Engineering*, pp. 799–810 (2017).
6. S. M. Liao and T. S. Zhao, "Measurements of Heat Transfer Coefficients From Supercritical Carbon Dioxide Flowing in Horizontal Mini/Micro Channels", *Journal of Heat Transfer* (3), pp. 413 (2002).
7. F. W. Dittus and L.M.K. Boelter, "Heat transfer in automobile radiators of the tubular type", *International Communications in Heat and Mass Transfer* 1, pp. 3–22 (1985).
8. C. Dang and E. Hihara, "In-tube cooling heat transfer of supercritical carbon dioxide. Part 1. Experimental measurement", *International Journal of Refrigeration* (7), pp. 736–747 (2004).
9. V. Gnielinski, "New equation for heat and mass transfer in turbulent pipe and channel flow", *International Chemical Engineering*, pp. 359–368 (1976).
10. J. D. Jackson and W. B. Hall, "FORCED CONVECTION HEAT TRANSFER TO FLUIDS AT SUPERCRITICAL PRESSURE", *Institution of Mechanical Engineers, Conference Publications* (1979).
11. A. Bruch; A. Bontemps; S. Colasson, "Experimental investigation of heat transfer of supercritical carbon dioxide flowing in a cooled vertical tube", *International Journal of Heat and Mass Transfer* (11-12), pp. 2589–2598 (2009).
12. W. Flaig; R. Mertz; J. Starflinger, "Design, control procedure and start-up of the sCO2 test facility SCARLETT", *DuEPublico, 2nd European sCO2 Conference 2018*, *2nd European sCO2 Conference 2018, Essen, Germany*, pp. 1–11 (2018).
13. J. Dirker and J. P. Meyer, "CONVECTION HEAT TRANSFER IN CONCENTRIC ANNULI", *Experimental Heat Transfer* 1, pp. 19–29 (2004).
14. Verein Deutscher Ingenieure, *VDI-Wärmeatlas* 11. ed., Springer Vieweg, Berlin (2013).

10.17185/duepublico/48882

DOI: 10.17185/duepublico/48882
URN: urn:nbn:de:hbz:464-20191004-132825-5